Observation of two-dimensional acoustic bound states in the continuum

Check for updates

Marc Martí-Sabaté[1,2], Junfei Li [ID][3], Bahram Djafari-Rouhani[4], Steven A. Cummer[5] & Dani Torrent [ID][1] [✉]

The design of devices based on acoustic or optical fields requires the fabrication of cavities and structures capable of efficiently trapping these waves. A special type of cavity can be designed to support resonances with a theoretically infinite quality factor, named bound states in the continuum or BICs. The experimental measurement of such modes is still a challenging problem, as they are, by definition, not accessible from external perturbations. Here we report on the theoretical design and experimental realization of a two-dimensional, fully open acoustic resonator supporting BICs. This accidental BIC, whose symmetry is chosen during design by properly tailoring the geometrical properties of the system, is completely accessible and allows for the direct measurement of the whole pressure field and properties. We experimentally demonstrate its existence with high quality factor and field enhancement properties.

Controlling the propagation and localization of waves is of paramount importance for a large number of modern applications based on the use of the energy or information carried out by these waves, including optical communications, quantum computing and sensing and imaging. One of the most efficient methods to achieve this control are the so-called embedded eigenstates, or bound states in the continuum (BICs), which have attracted great interest in recent years due to their many advantageous properties. BICs are modes in a system whose energy belongs to the radiation part of the spectrum while remaining spatially confined with an infinite lifetime. These modes were theoretically predicted just after the emergence of quantum mechanics by von Neumann and Wigner[1]. Since then, BICs have been designed and analyzed, resulting in different kinds and classifications for them, not only in quantum physics but also in photonics[2–8] and acoustics[9–14]. Their infinite quality factor makes them promising components of filters and resonators for classical waves, and for enhancing wave-matter interaction[15–18]. Their existence has been proved experimentally both in photonics[19–23] and acoustics[24–28].

Concerning acoustics, experimental measurements were first performed with a BIC created by a closed cavity attached to a one-dimensional waveguide by a small port[27]. This zero-dimensional BIC is enclosed within the cavity, and its quality factor was estimated through indirect measurements. Another experimental measurement was done using an open resonator embedded in a one-dimensional waveguide[29]. The quality factor was again estimated using the waveguide's transmission coefficient. Building upon this foundation, another experimental effort[26] employed two

separated cavities connected to a one-dimensional waveguide, in which the interaction between them creates a one-dimensional BIC (a Friedrich-Wintgen BIC in the case of the article). A recent work[30] has used Laser Doppler Vibrometer (LDV) measurements in order to visualize the acoustic field of a FW qBIC in a one-dimensional waveguide by using a transparent material for the cavity. By definition, BICs are confined and isolated from the rest of the system, implying that their excitation and measurement is not possible without altering the geometry by opening an input/output channel and thus leaking significant energy. Measuring directly the fields of a BIC mode is crucial to exploit the main characteristics of these systems; not only by their extreme confinement and its divergent quality factor, but also to probe the extreme field enhancement around their resonant frequency. This kind of measurement will open the field to real applications in which the properties of BICs will be actively exploited. Moreover, these previous efforts have been limited to zero- and one-dimensional acoustic BICs that do not exhibit the largely open boundaries that give BICs their most remarkable properties.

In this work we present the design of a two-dimensional fully open resonator that supports accidental BICs, and we fully characterize the BIC properties for acoustic waves by direct measurement. The system is formed by a set of precisely designed blind holes arranged as a regular polygon in a two-dimensional acoustic waveguide. The formation of such a mode can be explained by modelling the circular pattern of holes as a frequency-dependent impedance layer. This type of geometry has already been explored in photonics[31–35] explores the perturbation of the symmetry-

[1]GROC, UJI, Institut de Noves Tecnologies de la Imatge (INIT), Universitat Jaume I, 12071 Castelló de la Plana, Spain. [2]Department of Mathematics, Imperial College London, London SW7 2AZ, UK. [3]School of Mechanical Engineering, Purdue University, West Lafayette, IN 47907, USA. [4]IEMN, University of Lille, Cité scientifique, 59650 Villeneuve d'Ascq, France. [5]Department of Electrical and Computer Engineering, Duke University, Durham, NC 27708, USA. [✉]e-mail: dtorrent@uji.es

protected BICs of their circular structured unit cell under perturbation of the position of the resonators. In[32], an infinite space array of nanorods is studied, focused on the behavior of their system in the orthogonal plane to the nanorods axis. They distinguish two types of resonances, one of them being in the radiation regime, but not being a BIC because this kind of mode cannot exist in such a system (according to[36,37]). In[33,34] the same configuration is studied, comparing the modes that can be obtain in a one-dimensional grating with the ones that are obtained in this circular disposition of scatterers. Reference[33] considers propagation of waves in the plane orthogonal to the rods, while[34] also considers propagation in this direction, but in both cases BICs become qBICs in this circular geometry. Finally[35], is based on the existence of two different resonators in the circular array, with different resonant properties that cancel the radiative losses. The structure we propose is different to the ones studied in photonics since we are dealing with a waveguide, not with an open space. Thus, this structure is not subjected to the restriction found in[36,37].

By measuring the spatial distribution of the acoustic pressure field with fine frequency resolution, we obtain a complete picture of the BIC resonance, confirming good agreement between the designed and realized properties. Our basic BIC design is suitable for the generation of many multipolar modes, that might be foreseen useful for a broad range of applications based on the control of classical and quantum waves.

Results

Figure 1, panel a, shows the schematic view of the proposed structure supporting a 2D acoustic BIC. It consists in an acoustically rigid, structured bottom plate, and a flat glass top plate. The geometrical parameters that define this structure are the distance between the top and bottom plates (L) and the number N of identical blind holes of radius R_α and depth L_α drilled on the bottom plate and placed regularly along the perimeter of a circumference of radius R_0. Only half of the structure is shown in the figure, to illustrate the depth of the holes. This acoustic waveguide is designed to function within a mono-mode regime, specifically limited to the propagation of the fundamental mode within the frequency range of interest. This waveguide can be conceptualized as a two-dimensional space. However, the introduction of holes on the bottom surface disrupts the symmetry, leading to the excitation of a series of evanescent waves in the vicinity of these apertures.
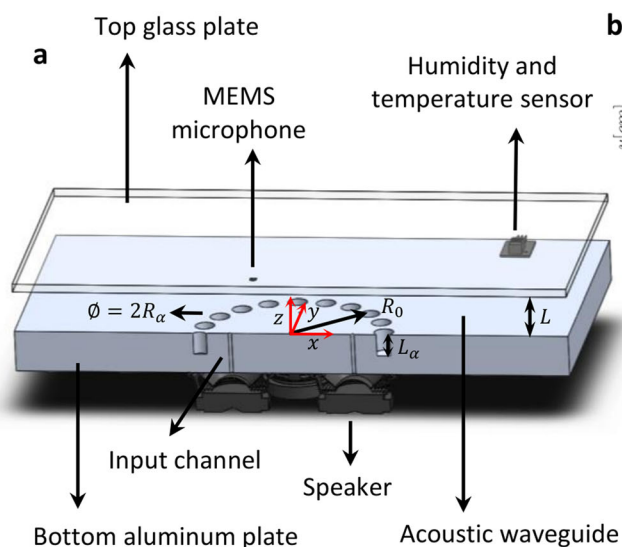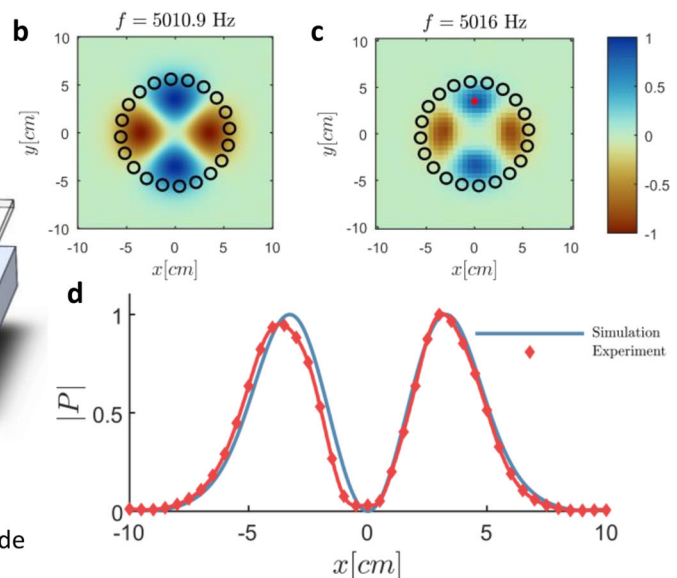
When these holes are arranged in a circular pattern, they collectively exhibit behavior akin to a frequency-dependent impedance layer, as explained in the supplementary note 3. This layer has the ability to function as either a perfectly rigid or soft wall, effectively confining waves within its boundaries. As will be shown below, by carefully selecting the frequency and adjusting the geometric parameters of the waveguide, a specific length for the holes can be identified. This optimal hole depth traps the chosen frequency within the cavity formed by the ring of holes, thereby defining a Bound State in the Continuum (BIC) for this two-dimensional space.

Circular clusters of scatterers have been studied in previous works to explore the presence of high quality modes for elastic[38–41] and electromagnetic waves[33–35], relating them to BICs. In this work, we realized the theoretical prediction, numerical validation, and the experimental characterization of acoustic BIC mode, depicted in panels **b** and **c**, respectively. The numerical prediction (**b**), is performed with COMSOL's Acoustic module frequency domain. The resonance frequency is obtained by sweeping in frequency and finding the frequency with the highest field amplitude. The experimental field shown in panel **c** depicts the pressure field distribution at the resonance frequency. The experimentally measured quality factor for this resonance is $Q = 182$. Panel **d** shows a cross section of panels **b** and **c** along the line $y = 0$. A good agreement is found between simulation and experimental measurements. Next section will show the physical principle and design process to obtain a resonant mode with an infinite quality factor (purely real eigenfrequency), obtaining then a BIC mode. We have employed a two-step approach. First, we built a theoretical model to calculate the geometrical parameters of both the holes and the plate. Then, finite element simulations using COMSOL have been done, fine tuning the parameters of the system to compensate the approximations in the analytical method, and studying the behavior of the mode under a more realistic environment. Finally, real experimental measurements have been conducted, and the experimental results will be shown and discussed.

2D BIC Design. The eigenfrequencies of the system shown in Fig. 1 can be found by the mode-matching method[42,43] as explained in detail in the supplementary notes 1 and 2. This method applies boundary conditions (continuity of pressure and normal velocity field) in the region of contact of two different domains (waveguide and cavities in our case) and simplify the system of equations by projecting the modes into another base of orthogonal

Fig. 1 | Designed bound state in the continuum (BIC) and achieved performance. Panel **a** shows an illustration of half of the designed plate, with its glass cover, placed at a distance L from the bottom layer. The speaker located at the bottom of the structure excites an acoustic field through the input channels, and it is recorded with a Micro-Electro-Mechanical System (MEMS) based microphone. The diameter of the holes is $2R_\alpha$ and their depth is L_α, and R_0 shows the radius of the circle where the holes are regularly placed. Panels **b** and **c** show the BIC normalized real pressure field in the plane $z = 0$, both in simulation (**b**) and in experiment (**c**) for a quadrupolar $\ell = 2$ mode. Panel **d** depicts the normalized absolute pressure field for the line $y = 0$, showing good agreement between simulation and experiment.

modes. The quality factor of an eigenmode is inversely proportional to the imaginary part of its eigenfrequency, thus we can define a BIC in acoustics as those modes having zero imaginary part in its eigenfrequency. For a cluster of holes drilled in an acoustically rigid cavity, a real eigenfrequency can be found as long as the following equation is satisfied

$$\cot(k_b L_\alpha) + 2N(-1)^\ell I_\ell(k_b) = 0, \tag{1}$$

with I_ℓ being

$$I_\ell(k_b) = \int_0^{+\infty} \frac{k_b}{q_k k} \cot(q_k L) J_\ell^2(kR_0) J_1^2(kR_\alpha) dk, \tag{2}$$

and R_α, L_α, R_0 and L being the radius and depth of the holes, the radius of the cluster and the height of the waveguide, respectively. The integer number ℓ is a label that defines the multipolar order of the mode (see equation (S15) in the supplementary note 1 for further details), $k_b = \omega/c_0$, c_0 is the speed of sound, and it has been set $c_0 = 344 m/s$ and $q_k = \sqrt{k_b^2 - k^2}$.

Equation (1) is a transcendental equation for the eigenfrequency $\omega = c_0 k_b$, consequently it is not efficient to select the geometry and then try to find the frequency at which the BIC is obtained. Instead, we can select the frequency at which we wish the BIC, then fix L, R_0 and R_α and, after the calculation of $I_\ell(k_b)$, we can use (1) to obtain L_α. As can be seen, $I_\ell(k_b)$ is always real, and the left hand side of equation (1) can take any value in the real axis, consequently one can always find a cluster dimension that corresponds to a BIC at any given frequency and for different multipoles for various values of ℓ.

The number of degrees of freedom, including the multipolar order of the mode, for this design is very large, however, if we want to obtain reasonable dimensions for the cluster that fits our experimental constraints, a systematic design of the cluster has to be done.

The approach that we followed allowed us to have a considerable control over the dimensions of the cluster. We begin by selecting the frequency at which we want the BIC to be found, which is $f_0 = 5$ kHz for experimental convenience. Next, selecting a symmetry of the field of $\ell = 2$, we set the radius R_0 of the cluster such that $k_b R_0$ is the argument of the first zero of the second order Bessel function, $j_{2,1} = 5.1356$. The reason for this choice is that it will minimize the field at the border of the cluster, so that we can expect that the quantity $I_\ell(k_b)$ will be small and then $k_b L_\alpha$ will be close to $\pi/2$, giving a reasonable size for the length L_α. Finally, we get $R_0 = 5.61 cm$.

Once the radius of the cluster has been selected, the radius of each hole can be established just by taking into account some constraints. The first constraint is about the maximum size of the radius of the hole. The distance between two adjacent holes in a circular cluster is $2R_0 \sin(\pi/N)$[40]; therefore, the radius is restricted to $R_\alpha < R_0 \sin(\pi/N)$ to avoid overlapping of the holes. Furthermore, if the radius of the holes is too large, the theoretical model developed here might fail, since we have used the mono-mode approximation in our equations, as explained in the supplementary notes 1 and 2. The second constraint involves the minimum size of the radius. If it is too small, in practice we will have very narrow channels for which the sound wave will be strongly dissipated, and the experimentally observed mode will have a poor quality. We have chosen $R_\alpha = 2/3R_0 \sin(\pi/N)$, so that the desired effect is produced. Selecting $N = 20$ we get $R_\alpha = 5.9$ mm. Finally, we select $L = 2.5 cm$ for practical reasons and equation (1) gives $L_\alpha = 1.36$ cm. Since the mode-matching method is not taking into account some evanescent fields near the surface of the holes, we choose to use the COMSOL simulations to compensate for it and find the exact solution for the BIC around the theoretically predicted value.

Equation (1) also shows that, for a given geometry of the cluster, changing the height of the waveguide will change the frequency of the mode. It also includes the uncovered scenario, in which we remove the top of the waveguide and have an open system. In this case, no BIC condition can be achieved, as explained in the supplementary note 1, however we also characterized experimentally this mode to measure its quality factor.

Numerical simulations and experimental results can be found in detail in the supplementary note 5, proving the existence of the resonance. For the covered case, after fine tuning the height of the plate (L), numerical simulations show a good agreement with the analytical design, as can be seen in Fig. 1 panel **b**. As expected, the field is contained in the inner part of the circle of holes, and the symmetry is the one given by the selected multipolar index ℓ.

Experimental measurements. Measurements were carried out to characterize the design experimentally and confirm the existence of a BIC, although in practice dissipation is always present and we have opened an inlet/outlet channel from the near field, which makes the mode present a finite quality factor. Experimental results show good agreement with predicted and simulated features. In Fig. 1, panels **b**, **c** and **d** prove that the scattering field at 5016 Hz looks the same as the one found in simulations, that is to say, to the designed BIC distribution. This excited field is completely confined inside the circle of radius R_0; the leakage of energy to the outside of the circle is evanescent, which means that these waves outside the circle do not carry energy to the far field. The experimental field shown in panel **c** is obtained from the real part of the Fourier transform of the field excited by a gaussian pulse with 5kHz center frequency, selecting the Fourier component which presents the highest amplitude.

Four speakers are placed under the aluminum bottom plate, oriented upwards. Four 2 mm diameter through holes are drilled on the bottom plate to channel energy from the speakers into the waveguide. The input signal to the speakers is a gaussian pulse centered at 5 kHz and spanning from 4 kHz to 6 kHz. The incident field is measured by covering up the blind holes, thus leaving a flat, empty waveguide with four deep-subwavelength through holes acting as point sources. The incident spectrum at the source point ($x = 0$, $y = 35$ mm, $z = 22$ mm, indicated in Fig. 1 panel **c** by a red dot) is shown in Fig. 2 panel **b**. The incident spectrum is different from a Gaussian shape, due to the non-uniform frequency response in the acoustic source, introduced by the holes in the plate, the speakers and the cavities behind them. The total field with BIC structure is then measured by uncovering the cluster of holes and sending in the same signal to the speakers. The scattered field is calculated as the total field subtracted by the incident field. More details about the experimental setup can be found in supplementary note 4.

When the cluster of holes is considered, the scattered field presents a sharp resonance at 5016 Hz. Figure 2 panel b shows the two normalized spectra. The relative amplitude at other frequencies is much lower than the resonance. The temporal signal in panel **a** also agrees with this interpretation. The duration of the incident pulse is less than 5 ms at the measurement position, while the scattered field rings at least 50 ms. The temporal envelope, together with the narrow spectral content, states that the mode at 5 kHz is excited and retained in the inner part of the cluster for a long time, as can be seen in the video of the supplementary movies 1 and 2. Such a long ringing time allows us to directly measure the quality factor, instead of calculating FWHM. The black curve in Fig. 2 panel a shows the fitting of the curve by a decaying exponential ($x(t) = Ae^{-\omega_i t}$). The quality factor is then estimated as $Q = \omega_0/2\omega_i$, where ω_0 is the resonant frequency and ω_i is the imaginary frequency term. In the example shown in the figure, the measured Q is 172. The quality factor should be independent of the position at which the measurement is done; in fact, we have measured many other points to confirm that the estimation of the quality factor is consistent.

Figure 2 panel c shows the ratio between the scattered and incident spectrum. There is a sharp peak around the 5 kHz, signifying a substantial sensitivity enhancement, approximately twenty-five times larger. Such a feature makes our BIC structure particularly appealing for sensing applications. The measured acoustic field at peak frequency, shown in Fig. 1 panel **c**, demonstrates almost perfect agreement with the theoretical prediction.

Mode's robustness

A valuable property of the system studied in this work is its easy reconfigurability, since the BIC condition strongly depends on the geometrical parameters of the waveguide and the cluster, which means that the quality factor can be easily controlled by adjusting the geometry, such as the height

Fig. 2 | **Experimental results obtained for the** $\ell = 2$ **designed plate.** Panel **a** shows the incident and the scattered signal and envelope at a given point ($x = 0$, $y = 35$ mm, $z = 22$ mm). The black line is the fitting by a decaying exponential used to estimate the quality factor of the resonance. Panel **b** shows the spectra of both signals in normalized units. Panel **c** shows the ratio between the scattered spectrum and the input spectrum. A peak at 5015 Hz is seen, showing an energy enhancement at this frequency due to the presence of the cluster of holes.
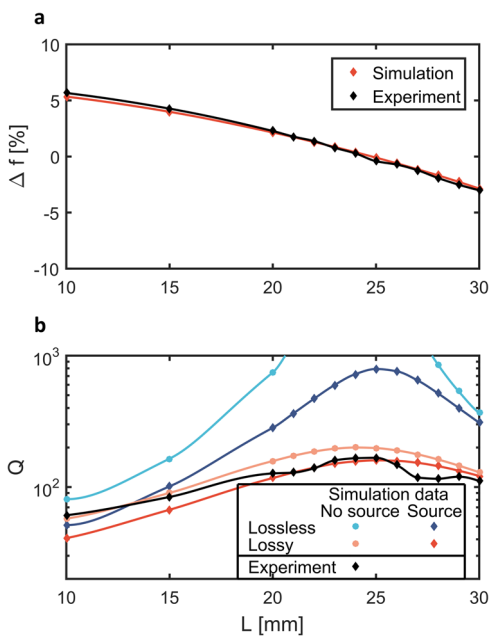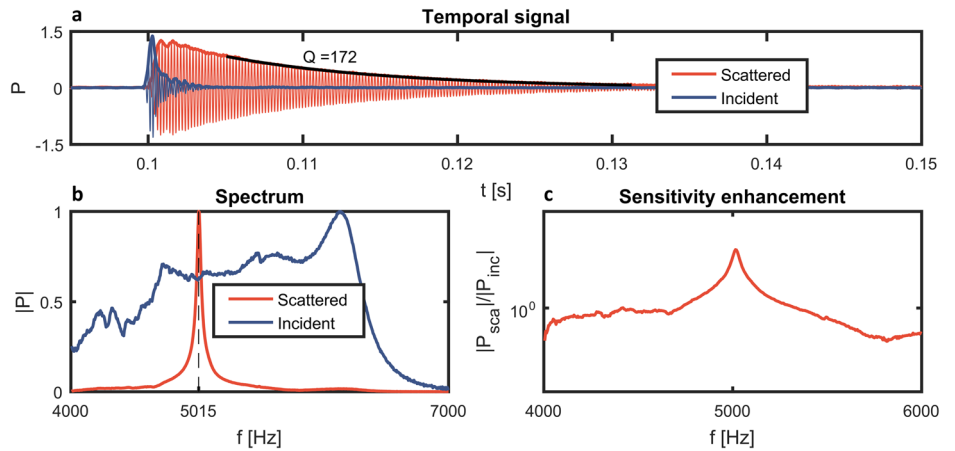
Fig. 3 | **Experimental evolution of the mode with changing geometrical parameters. a** Dependence of the resonant frequency of the mode with the height L of the cavity keeping all the other geometrical parameters fixed. **b** Quality factor of the resonance as a function of the covered plate distance. Black rhombus represent the experimental results, while the rest of data is simulation, considering lossy or lossless material and considering the presence of the input channel in the system. As can be seen, the quality factor of the BIC is far from being infinite, and the two loss mechanisms (lossy material and input channel) explain the behavior of the experimental results.

of the waveguide (L). Figure 3 panel a shows the evolution of the resonant frequency of the mode with the height L of the cavity. As we see, the relative variation of the eigenfrequency is very small, although the quality factor strongly depends on this parameter, as explained below.

Figure 3 panel b shows the evolution of the quality factor as a function of the height of the waveguide L for the $\ell = 2$ mode. The experimental results are depicted in black. The quality factor is not divergent as we approach the theoretically predicted BIC, due to the unavoidable dissipation in the real system. Nevertheless, it is shown that these results match the ones found in simulation considering losses in the material and in the excitation system. Loss in material is modeled by adding imaginary part to the sound speed $c = c_0(1 + 0.0025i)$. Loss in the excitation system is modeled by considering cylindrical wave radiation boundary condition at the bottom surface of the 4

input channels. Blue dots represent the simulation values obtained from eigenfrequency simulations considering no losses in the material and no losses due to the excitation system. It is seen that, in the interval from $L = 21$ mm to $L = 26$ mm, the quality factor is higher than 1000. A real eigenvalue (and thus, an infinite quality factor) can be found for $L = 24$ mm. The range in the figure has been limited to better illustrate the shape of the curves considering noise. Blue diamonds in Fig. 3 panel b represent eigenfrequency simulations considering no losses in the material, but losses in the excitation system. The results show that the quality factor cannot reach an infinite value as in the previous case; the quality factor will always remain under 1000. The maximum is now found for $L = 25mm$ ($Q = 792$). This result agrees with what is known about BICs; ideally, they are states whose energy remains confined for an infinite lifetime, without leakage into the bulk. The system we are working with is reciprocal, meaning that, neither the energy can be leaked to the outside, nor the energy coming from the outside will excite the BIC. Thus, the mode is completely isolated from the outside. In real life, in order to achieve the excitation of the state, an input/output channel must be created. In the case of this experiment, this is the role of the four holes located in the interior of the circle and connecting the top and bottom surface of the aluminum plate, where the speakers are placed. The energy is then able to flow from the speakers into the waveguide, where the BIC mode will be excited. Consequently, these channels will allow small energy leakage from the inside the cluster to the outside.

Red dots in Fig. 3 panel b represent eigenfrequency simulations with material loss but without considering leakage from the excitation system. The quality factor threshold is even lower than in the previous case, indicating that loss mechanism in air is more crucial than the loss introduced by the source, even if the percentage of losses in air has been estimated to be very low ($0.25\%c_0 = 0.86m/s$). Finally, red diamonds in Fig. 3 panel **b** represent eigenfrequency simulations with both loss mechanisms. Experimental results match the simulations when loss in both material and excitation system are considered. They have been measured under the following environmental conditions: $T = 21.5°C$ and $HR = 10\%$ (humidity rate). According to[44], decreasing the temperature or increasing the humidity could further reduce the inherent loss in air. In our experiment, by using a humidifier near the waveguide to increase the humidity, we have measured $Q = 182$ at $T = 21.5°C$ and $HR = 40\%$.

The effect of the variation of other geometrical parameters can be analysed in the system. Figure 4, panels a–c show the dependence of the central frequency as a function of the different geometrical parameters of the structure, while panels d–f depict the same dependence but for the quality factor of the modes. We see from panels a and d how these two parameters depend on the radius of the holes (R_a). Two different colours are displayed: red lines correspond to lossless simulations without the excitation system (the four throughout holes). Black lines represent lossless simulations with the excitation holes. The y axis in the quality factor graph has been limited to
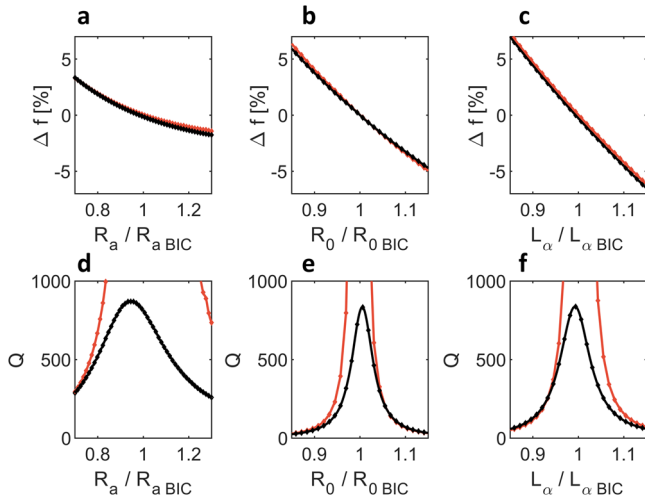
Fig. 4 | Evolution of the central frequency and the quality factor of a BIC as a function of geometrical parameters of the system. Panels **a**–**c** correspond to the variation of the central frequency as a function of the radius of the holes, the cluster and the length of the holes, respectively. Similarly, panels **d**–**f** show the variation of the quality factor of the resonance as a function of the radius of the holes, the cluster and the length of the holes, respectively.

1000 in order to get a better idea of the performance with the excitation system, which is more accurate. As for the red line, it goes up to infinite at the exact geometrical configuration of the BIC ($R_a/R_{aBIC} = 1$). We can clearly see that the resonance still exists at configurations other than the BIC conditions. Its central frequency is shifted and its quality factor quickly decays, but it is measurable. The same analysis is repeated in panels b and e for the performance of the device when the radius of the cluster changes (R_0). In this case, the radius of the holes has been kept constant. The conclusions are similar to the previous ones, except that in this case the relative variation of the geometrical parameter is smaller, with a higher reduction in the quality factor. This means that the BIC performance is more sensitive to a variation of the radius of the circle of resonators rather than the radius of the resonators themselves. Panels c and f show the behavior of the system as a function of the variation of the depth of the holes (L_α). The results are similar to the variation of R_0; that is to say, the device it is more sensitive to L_α than to R_a variations.

Other experimental measurements concerning the robustness of the device are shown in Fig. 5. Panels a–c show results for the case in which one hole has been removed from the system. It is removed by adding a piece of material that covers the whole hole. This material (polylactic acid, PLA) has been considered stiff enough, so that no acoustic field propagates inside the material. Panel a shows the field distribution of the experimentally measured $\ell = 2$ mode for the original structure (all the holes are present in the cluster). However, the illustration shows one missing hole in the structure. This is the default considered in panel b, where different spectra have been depicted. Instead of measuring all the field positions, the effect of the default in the mode has been evaluated by measuring the response at the four points labeled in panel a by four colour points (orange, red, green and blue). Dotted lines in panel b correspond to the whole structure scenario, where all the holes are present. The spectral response is almost the same for the four measured points. Full lines show the behaviour of the system when there is a hole missing. The shape of the spectra is almost the same, but there is a clear reduction in the frequency peak. This peak reduction is the chosen parameter for panel c; it shows the frequency peak reduction as a function of the position of the missing hole of the cluster. As it can be seen, this peak reduction also presents an $\ell = 2$ symmetry; when the missing hole is placed near a zero pressure point of the original mode, the influence of the default is negligible (so the parameter $|p_{default}|/|p_{original}|$ tends to one). Nevertheless, when the missing hole is near one maximum or minimum of the mode, its

influence is higher, and a peak reduction is appreciated. The four colours represent the four measured positions, but they all have the same behaviour.

Panels d and e in Fig. 5 show the scenario in which more than one hole is removed in the cluster. The holes are not removed randomly; instead, it is always deleted one hole adjacent to the last hole removed, such that the opening of the cluster to the rest of the plate increases, as can be seen in panel d. Panel e shows the temporal evolution of the envelope of the signal, measured at $x = 3.5$ cm, $y = 0$ cm, $z = 2.2$ cm. From the graph, it can be seen that the temporal response becomes shorter as the number of removed holes from the structure increases, indicating a decrease in the quality factor of the mode. Quantitatively, the quality factor for the original structure is $Q = 172$. When the first hole is removed, the quality factor gets reduced to $Q = 126$. Remember that the position of the first missing hole is of paramount importance (Fig. 5 panel **c**). In this case, the first hole removed is placed at the most critical position, that is to say, the one that presents a bigger reduction of the frequency peak, and thus, of the quality factor. For the rest of scenarios, the quality factors are $Q = 44$, $Q = 61$, $Q = 39$ and $Q = 12$. The quality factor decreases with the number of holes removed (except for the case 2 and 3).

Conclusions

In summary, we have designed and experimentally measured an acoustic two-dimensional open resonator supporting the existence of a family of bound states in the continuum (BICs) in circular arrays of scatterers. Its performance depends on the geometrical parameters of the configuration, and can be easily tuned numerically. Our approach allows us to confine the acoustic field in a fully open space in a two-dimensional waveguide instead of inside a closed cavity, and it is robust enough to allow for the direct measurement of the field inside the waveguide without destroying the resonance. Experimental measurements agree with simulations; the pressure field is contained by the structure and there is no leakage of energy to the waveguide. Furthermore, the existence of the BIC is linked to the field enhancement at the mode frequency. Results show that the energy density is increased by more than two orders of magnitude at the BIC frequency. The maximum measured quality factor is 182; this result matches with what is found in simulation and it is consistent with the loss mechanisms that exist in the system, which is dominated by intrinsic acoustic losses in air.

The properties of our design may find applications in enhanced acoustic emissions, and might be suitable for the design of acoustic filters and sensors. Also, the results shown here were previously theoretically demonstrated for elastic and optical waves, consequently a properly designed system could be used for the simultaneous control of different wave fields or even to enhance the interaction between them.

Methods
Numerical simulations
The full wave simulations based on finite element analysis are performed using COMSOL Multiphysics Pressure Acoustics module. The simulated domain is a cylinder with radius $R_{cyl} = 3R_0$. For the uncovered plate scenario, perfectly matched layers are adopted in the top boundary to reduce reflections, while plane wave radiation boundary conditions are applied on the sides to simulate the propagation to an infinite system. In the covered case, the perfectly matched layer is substituted by a rigid boundary condition at the height of the top plane. Speed of sound is 344 m/s (after measurement in the laboratory). Losses have been simulated by adding an imaginary component to the speed of sound. Furthermore, losses in the input channel have been simulated by applying cylindrical wave radiation boundary conditions in the bottom surface of the throughout holes connecting the bottom and top surface of the bottom plate. All boundaries between air and solid (glass or aluminium) have been considered rigid.

Experimental apparatus
The sample was fabricated by drilling twenty blind holes in aluminum with a CNC machine. The size of the plate is $18 \times 18 \times 1$ inch. The diameter of the
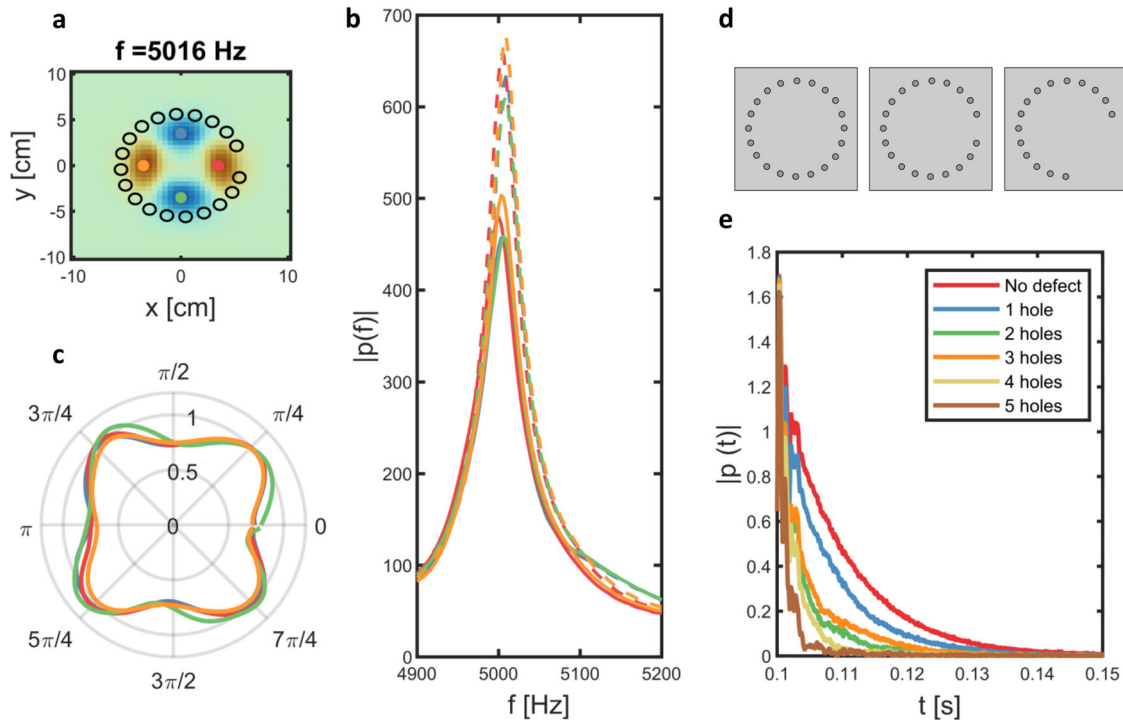
Fig. 5 | BIC robustness under defaults. Panel **a** shows the energy distribution for a $\ell = 2$ mode with all the holes in the structrue (original cluster). The illustration showing the holes in the cluster, however, has one missing hole, indicating the position of the hole missing for panel **b**. Colour points (orange, green, blue and red) indicate the position of the measured points for the other panels. Panel **b** shows the spectra of the measured points, both for the original cluster (dotted lines) and for the missing hole scenario (full lines). Panel **c** shows the ratio between the spectrum coefficient at 5016 Hz (which corresponds to the mode) for the missing hole scenario and the original one. The angle in this graph indicates the position of the missing hole. Illustration **d** shows the picture of the plate for three different cases, in which we have been successively removing holes from the cluster. The third picture has five consecutive holes missing. Panel **e** shows the temporal envelope of the signal measured at the point $x = 3.5$ cm.

holes is 1/2 inch. The four throughout holes corresponding to the input energy channels have also been drilled using a CNC machine. In this case, the diameter is 5/64 inch (~2 mm). A 1-inch speaker is attached to the end of each through hole, acting as the sound source. Four speakers have been used as excitation system, driven by a 4-channel audio power amplifier and a Multifunction I/O card (National Instruments PCIe 6353) emitting pulses centered at 5 kHz and spanning from 4 kHz to 6 kHz. For calibration, the amplitude of each speaker has been normalized to obtain the same spectral response on top of the speaker. Four 3D printed ABS plastic pillars have been used at the corners of the glass plate to support its weight, forming a 2D waveguide between the bottom aluminum plate and top glass plate. The wedge shaped acoustic foams are sandwiched between two plates at the four edges of the waveguide to eliminate reflection. A picture of the system setup is shown in Supplementary Fig. 2.

The pressure field inside the waveguide was measured with a MEMS microphone (SparkFun ADMP401). A pair of magnets is attached to the speaker and the scanning stage, so the microphone inside the waveguide follows the movement of the scanning stage outside the waveguide. The signal is then collected by a DAQ (National Instruments PCIe 6353). The same experiment has been repeated when the microphone scans the measurement area, and the acoustic field is then synthesized by combining the detected signals at each microphone position. The overall scanned area is 10 cm by 10 cm grid with a step of 0.5 cm. At each position, the experiment is repeated ten times and the resulting signal is time-averaged in order to reduce noise.

Measurements shown here have been done under laboratory environmental conditions ($T = 21.5\,°C$ and $HR = 10\%$). The edge of the structure is surrounded by wedge-shaped acoustic foam to mimic an anechoic environment, and the detected signals are time-gated to eliminate reflection. Frequency domain field plots are obtained through the Fourier transform of the time-domain signals at each point, and the scanned acoustic field is

visualized by plotting the real part of the field at the target frequency. The scattered field is measured as the difference between the total field (with the cluster), and incident field (without the cluster). The temperature and humidity of the experiment environment is measured by an indoor humidity thermometer, placed inside the 2D waveguide close to the foam. Since the acoustic field of BIC is tightly confined in the center region, the thermometer placed on the edge of the waveguide does not affect the field.

Data availability
The data that support the findings of this study are available from the corresponding author on reasonable request.

References
1. Neumann, J. V. & Wigner, E. P. Über merkwürdige diskrete eigenwerte, *Phys. Z.* **30**, 291–293 (1929).
2. Molina, M. I., Miroshnichenko, A. E. & Kivshar, Y. S. Surface bound states in the continuum. *Phys. Rev. Lett.* **108**, 070401 (2012).
3. Miroshnichenko, A. E., Flach, S. & Kivshar, Y. S. Fano resonances in nanoscale structures. *Rev. Mod. Phys.* **82**, 2257 (2010).
4. Hsu, C. W., Zhen, B., Stone, A. D., Joannopoulos, J. D. & Soljačić, M. Bound states in the continuum. *Nat. Rev. Mater.* **1**, 1 (2016).
5. Hsu, C. W. et al. Bloch surface eigenstates within the radiation continuum. *Light Sci. Appl.* **2**, e84 (2013).
6. Sadreev, A. F. Interference traps waves in an open system: bound states in the continuum. *Rep. Prog. Phys.* **84**, 055901 (2021).
7. Bulgakov, E. N. & Sadreev, A. F. Bound states in the continuum in photonic waveguides inspired by defects. *Phys. Rev. B* **78**, 075105 (2008).

8. Zhen, B., Hsu, C. W., Lu, L., Stone, A. D. & Soljačić, M. Topological nature of optical bound states in the continuum. *Phys. Rev. Lett.* **113**, 257401 (2014).

9. Friedrich, H. & Wintgen, D. Interfering resonances and bound states in the continuum. *Phys. Rev. A* **32**, 3231 (1985).

10. Huang, L. et al. General framework of bound states in the continuum in an open acoustic resonator. *Phys. Rev. Appl.* **18**, 054021 (2022).

11. Quotane, I. et al. Trapped-mode-induced fano resonance and acoustical transparency in a one-dimensional solid-fluid phononic crystal. *Phys. Rev. B* **97**, 024304 (2018).

12. Jin, Y., Boudouti, E. H. E., Pennec, Y. & Djafari-Rouhani, B. Tunable fano resonances of lamb modes in a pillared metasurface. *J. Phys. D: Appl. Phys.* **50**, 425304 (2017).

13. Mizuno, S. Fano resonances and bound states in the continuum in a simple phononic system. *Appl. Phys. Express* **12**, 035504 (2019).

14. Sadreev, A., Bulgakov, E., Pilipchuk, A., Miroshnichenko, A. & Huang, L. Degenerate bound states in the continuum in square and triangular open acoustic resonators. *Phys. Rev. B* **106**, 085404 (2022).

15. Kodigala, A. et al. Lasing action from photonic bound states in continuum. *Nature* **541**, 196 (2017).

16. Koshelev, K., Bogdanov, A. & Kivshar, Y. Meta-optics and bound states in the continuum. *Science Bulletin* **64**, 836 (2019).

17. Wu, M. et al. Room-temperature lasing in colloidal nanoplatelets via mie-resonant bound states in the continuum. *Nano Lett.* **20**, 6005 (2020).

18. Koshelev, K. et al. Subwavelength dielectric resonators for nonlinear nanophotonics. *Science* **367**, 288 (2020).

19. Gansch, R. et al. Measurement of bound states in the continuum by a detector embedded in a photonic crystal. *Light Sci. Appl.* **5**, e16147 (2016).

20. Capasso, F. et al. Observation of an electronic bound state above a potential well. *Nature* **358**, 565 (1992).

21. Plotnik, Y. et al. Experimental observation of optical bound states in the continuum. *Phys. Rev. Lett.* **107**, 183901 (2011).

22. Shi, T. et al. Planar chiral metasurfaces with maximal and tunable chiroptical response driven by bound states in the continuum. *Nat. Commun.* **13**, 4111 (2022).

23. Chen, Y. et al. Observation of intrinsic chiral bound states in the continuum. *Nature* **613**, 474 (2023).

24. Cobelli, P., Pagneux, V., Maurel, A. & Petitjeans, P. Experimental observation of trapped modes in a water wave channel. *Europhys. Lett.* **88**, 20006 (2009).

25. Huang, S. et al. Extreme sound confinement from quasibound states in the continuum. *Phys. Rev. Appl.* **14**, 021001 (2020).

26. Huang, L. et al. Topological supercavity resonances in the finite system. *Adv. Sci.* **9**, 2200257 (2022).

27. Huang, L. et al. Sound trapping in an open resonator. *Nat. Commun.* **12**, 1 (2021).

28. Amrani, M. et al. Experimental evidence of the existence of bound states in the continuum and fano resonances in solid-liquid layered media. *Phys. Rev. Appl.* **15**, 054046 (2021).

29. Jia, B. et al. Bound states in the continuum protected by reduced symmetry of three-dimensional open acoustic resonators. *Phys. Rev. Appl.* **19**, 054001 (2023).

30. Kronowetter, F. et al. Realistic prediction and engineering of high-q modes to implement stable fano resonances in acoustic devices. *Nat. Commun.* **14**, 6847 (2023).

31. Meng, B., Wang, J., Zhou, C. & Huang, L. Bound states in the continuum supported by silicon oligomer metasurfaces. *Opt. Lett.* **47**, 1549 (2022).

32. Han, H.-L., Li, H., bin Lü, H. & Liu, X. Trapped modes with extremely high quality factor in a circular array of dielectric nanorods. *Opt. Lett.* **43**, 5403 (2018).

33. Bulgakov, E. N. & Sadreev, A. F. Nearly bound states in the radiation continuum in a circular array of dielectric rods. *Phys. Rev. A* **97**, 033834 (2018).

34. Bulgakov, E. & Sadreev, A. Fibers based on propagating bound states in the continuum. *Phys. Rev. B* **98**, 085301 (2018).

35. Kühner, L. et al. Radial bound states in the continuum for polarization-invariant nanophotonics. *Nat. Commun.* **13**, 1 (2022).

36. Colton, D. L., Kress, R. and Kress, R., *Inverse acoustic and electromagnetic scattering theory*, Vol. 93 (Springer, 1998).

37. Silveirinha, M. G. Trapping light in open plasmonic nanostructures. *Phys. Rev. A* **89**, 023813 (2014).

38. Movchan, A., McPhedran, R., Carta, G. & Craster, R. Platonic localisation: one ring to bind them. *Arch. Appl. Mech.* **89**, 521 (2019).

39. Putley, H., Chaplain, G., Rakotoarimanga-Andrianjaka, H., Maling, B. & Craster, R. Whispering-bloch elastic circuits. *Wave Motion* **105**, 102755 (2021).

40. Martí-Sabaté, M., Djafari-Rouhani, B. & Torrent, D. Bound states in the continuum in circular clusters of scatterers. *Phys. Rev. Res.* **5**, 013131 (2023).

41. Movchan, A. B., McPhedran, R. C. & Carta, G. Scattering reduction and resonant trapping of flexural waves: Two rings to rule them, *Appl. Sci.* **11**, https://doi.org/10.3390/app11104462 (2021).

42. Torrent, D. Acoustic anomalous reflectors based on diffraction grating engineering. *Phys. Rev. B* **98**, 060101 (2018).

43. Torrent, D. & Sánchez-Dehesa, J. Acoustic analogue of graphene: Observation of dirac cones in acoustic surface waves. *Phys. Rev. Lett.* **108**, 174301 (2012).

44. Harris, C. M. Absorption of sound in air versus humidity and temperature. *J. Acoust. Soc. Am.* **40**, 148 (1966).

Acknowledgements

Author contributions

D.T., B.D.R. and M.M.S. conceived the idea and developed the theoretical analysis. J.L., M.M.S. and S.C. performed the experimental demonstration. All authors contributed equally to the manuscript writing.

Competing interests

The authors declare no competing interests.

Additional information

Supplementary information The online version contains supplementary material available at https://doi.org/10.1038/s42005-024-01615-8.

Correspondence and requests for materials should be addressed to Dani Torrent.

Peer review information *Communications Physics* thanks the anonymous reviewers for their contribution to the peer review of this work.

Reprints and permissions information is available at http://www.nature.com/reprints

Publisher's note Springer Nature remains neutral with regard to jurisdictional claims in published maps and institutional affiliations.